Simulations of a DIII-D Plasma Disruption with the NIMROD Code

S.E. Kruger 1), D.D. Schnack 2),

1) Tech-X Corporation, Boulder, CO, USA
2) SAIC, San Diego, California, USA

email contact: krugers@saic.com

Abstract. [**?**] Two simulations with the NIMROD code [**?**] that model DIII-D discharge 87009 are presented. In the first simulation, a fixed-boundary equilibrium is used to model the physics of a plasma being heated through an ideal magnetohydrodynamic (MHD) instability threshold. This simulation shows a faster than exponential increase in magnetic energy as predicted by analytic theory [1]. The second simulation starts from an equilibrium that has the plasma beta raised 8.7% above the best equilibrium reconstruction to start above the ideal MHD threshold. The nonlinear evolution of the ideal mode leads to a stochastic magnetic field and parallel heat transport leads to a localization of the heat flux that is deposited on the wall. The structure of the heat flux deposition is dependent upon the magnetic topology which results from the growth of the ideal mode.

I. INTRODUCTION

During tokamak experimental operation, events which rapidly terminate the plasma discharge occasionally occurs. The complete and rapid loss of thermal and magnetic energy in these disruptions result in large thermal and magnetic loads on the material wall. For proposed next step experiments such as the International Thermonuclear Experimental Reactor (ITER), the stored energy will be approximately 100 times greater than present day devices, which presents many engineering challenges. Exacerbating the difficulties, the disruption phenomena is often highly non-axisymmetric [1] resulting in localized deposition of the heat loads. Understanding the onset mechanisms and the nonlinear dynamics leading to the disruption is crucial for understanding ways to prevent or mitigate disruptions.

The experimental phenomenology of the disruption in DIII-D discharge 87009 has attracted a great deal of theoretical interest [2-5]. A combination of analytic theory [2] and linear ideal

MHD code analysis [3] has been successful in predicting both the time scale of the disruption [2] and the spatial structure [3] of the mode. The success of the model and the indication that the phenomenology can be described with strictly a magnetohydrodynamic model makes this an attractive case to study with the NIMROD [6] nonlinear initial-value code. Unlike the simple analytic/linear numerical MHD model, an initial-value code allows for detailed studies of the mechanism leading to the loss of plasma confinement and the resultant heat deposition on the plasma wall.

This paper presents two different NIMROD simulations. In the first, the time-dependent behavior is modeled using a fixed boundary equilibria. The emphasis of this simulation is to numerically verify the analytic model of Reference [1]. In the second simulation, the NIMROD simulation starts from a free-boundary equilibrium that is above the ideal MHD threshold. The emphasis in this simulation is to model how the heat flux gets deposited on the wall. In the final section, conclusions are drawn and further work is discussed.

II. FIXED-BOUNDARY SIMULATIONS

Long wavelength instabilities in fusion plasmas have often been described within the framework of magnetohydrodynamic (MHD) theory. These instabilities are often categorized by the physics in the generalized Ohm's law required for the instability to be described (e.g. ideal, resistive, neoclassical), as described in Appendix A. The types of instabilities have different time scales associated with their growth, with the ideal modes growing on the Alfvenic time scale, and the other modes having a time scale that is a hybrid of the Alfvenic and resistive time scales.

In using MHD theory to understand experimental observations of these long-wavelength modes, the marginal stability point as calculated by linear eigenvalue codes is frequently the primary determination of theory-experimental comparisons [2]. However, for experimental and computational studies, the variation of the growth rate away from the critical point is also an important parameter as is heuristically shown in Figure 1, where we consider the growth rate as a function of β.

If we assume that the mode grows with an exponential growth from an initial amplitude, ξ_0, to one where it is large enough to be observed, ξ_{obs}, then any growth rate that is less than a critical parameter

$$\gamma_{exp} = \frac{1}{\tau_{exp}} \ln \frac{\xi_0}{\xi_{obs}}, \tag{1}$$

where $\tau_{\rm exp}$ is the duration of the experiment from mode onset, is *experimentally stable*. As shown in Figure 1, the operating range in β that the experimentally stable regime increases, as compared to the exact marginal stability point, depends on the variation of the growth rate with the free energy which is characterized by $\hat{\gamma}_{MHD}$ [1] (using a Taylor expansion about the marginal point).

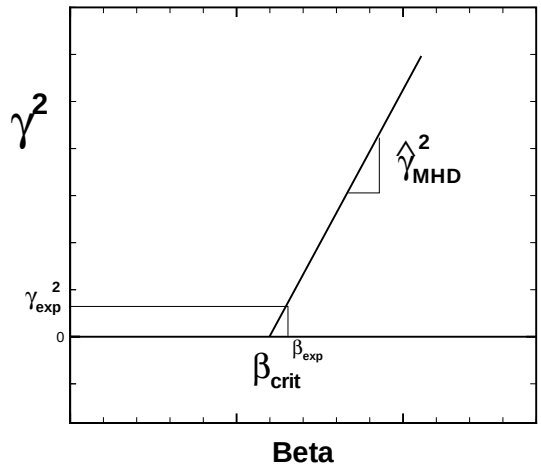

FIG. 1: The variation of growth rate with free energy, as parameterized by $\hat{\gamma}_{MHD}$, is nearly as important as the location of the marginal point in interpreting experimental results.

This analysis however neglects how the plasma reached an unstable equilibrium. Recently, an analytic theory [1] has been put forth to describe the growth of an instability being driven through the marginal stability point. Assuming that the free energy of the mode is proportional to β, then

$$\omega^2 = \frac{\delta W}{\delta K} \sim -\hat{\gamma}^2_{MHD}\left(\frac{\beta}{\beta_{crit}} - 1\right). \tag{2}$$

Assuming a slow heating rate so that the heating may be approximated as a linear increase in β with a heating rate γ_h near the marginal point, $\beta(t) = \beta_{crit}(1+\gamma_h t)$, one obtains a growth rate that depends on the heating rate with the resultant mode growing faster than exponential:

$$\xi = \xi_0 \exp\left[(t/\tau)^{3/2}\right]. \tag{3}$$

The time constant of the mode is a hybrid of the variation of the growth rate with beta and the heating time scale:

$$\tau \equiv \frac{(3/2)^{2/3}}{(\hat{\gamma}_{MHD})^{2/3}\gamma_h^{1/3}}. \tag{4}$$

As the limit of either $\hat{\gamma}_{MHD}$ or γ_h goes to zero, the mode does not grow because it is exactly at the marginal point.

This heuristic analytic theory was successfully used to explain many of the features of DIII-D discharge 87009 which disrupted during neutral-beam heating [1]. To further test this theory and gain additional insight into the nonlinear behavior, discharge 87009 was modeled using the nonlinear resistive MHD equations with anisotropic heat conduction (see Appendix A) with an equilibrium with similar pressure and safety factor profiles as the actual discharge at 1681.7 msec, but with the plasma pressure raised to the ideal marginal stability point when a conducting wall is placed on the last closed flux surface.

Before running a self-consistent nonlinear simulation with heating, it is necessary to begin the simulation near the ideal marginal stability point. To determine the critical beta with sufficient accuracy, the equilibrium was varied from $\beta_N = 4.0$ to $\beta_N = 5.0$ in increments of $\Delta\beta_N = 0.05$. The ideal linear stability of the equilibria was tested with DCON [3] to determine plasma stability to ideal modes using a generalized version of Newcomb's criterion [4]. Because linear calculations with NIMROD take much longer than DCON to determine ideal stability, using DCON on a large number of equilibria is generally preferred. The ideal marginal stability point was found by DCON to be $\beta_N = 4.45$. Linear NIMROD simulations found resistive interchange modes at $\beta_N = 4.0$, and the extremely robust growth rates expected of ideal instabilities at $\beta_N = 5.0$ and $\beta_N = 6.0$ as shown in Figure 2. Because the growth of the mode at $\beta_N = 4.45$ is very slow, we consider it to be *computationally stable* (with regards to ideal instabilities) and we chose $\beta_N = 4.70$ as the starting point for our calculations.

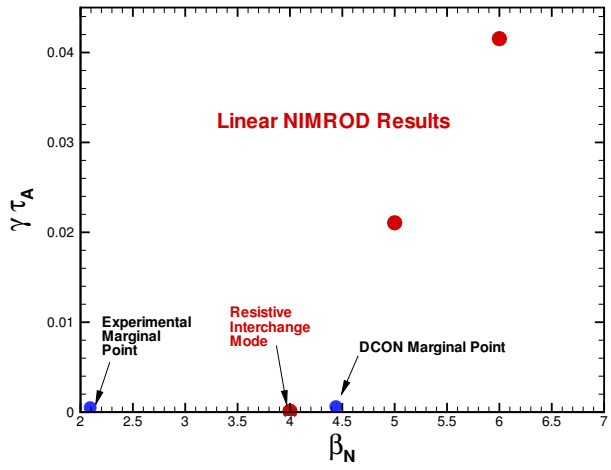

FIG. 2: Linear NIMROD runs used in conjunction with DCON determine the marginal stability point with pressure that is larger than the experiment. Nonlinear NIMROD runs started with an equilibrium at $\beta_N = 4.70$.

To model the heating of the plasma, we apply a heating source that increases the equilibrium pressure self-similarly

$$\frac{\partial p}{\partial t} = ... + \gamma_h p_{eq}. \tag{5}$$

As the plasma heats, the flux surfaces shift outward, but the heating is still be peaked at the old magnetic axis. Because our heating rate is slow compared to the growth of the mode, but still much faster than the resistive decay time ($\hat{\gamma}_{MHD} \gg \gamma_h \gg 1/\tau_R$), the assumptions of the analytic theory [1] are satisfied. Note that throughout the simulations, NIMROD's finite-element grid is aligned to the equilibrium magnetic field and does not move.

The NIMROD simulations were run with Lundquist number, $S = 10^6$, Prandtl number (ratio of normalized resistivity to kinematic viscosity) $Pr = 200$ with heating rates of $\gamma_h = 10^{-3}\ s^{-1}$ and $\gamma_h = 10^{-2}\ s^{-1}$. A finite-element grid in the poloidal plane with 128 radial vertexes and 64 poloidal vertexes was used with cubic polynomial Lagrangian elements [5]. The toroidal direction is discretized using the pseudo-spectral method using the $n = 0$ and $n = 1$ modes. Because the vacuum region is not included in these simulations, the increase in beta to make the $n = 1$ mode unstable results in the higher n modes to be substantially destabilized. Because two-fluid effects stabilize these modes but introduce a substantial time step limitation due to the dispersive Whistler wave, only the first two modes are kept. Our results are only qualitatively correct in the fully nonlinear regime, but the goal is to compare with the quasi-linear analytic theory. The results of a NIMROD simulations with $\gamma_h = 10^{-3}\ s^{-1}$ are shown in Figure 3. As predicted by the analytic theory, the growth of the mode is faster than exponential. As represented by the straight lines in the fitting shown in Figure 4, the growths satisfy Eq. (3) well into the nonlinear regime. Using the slopes of the lines in Figure 4 to determine the time constant for each heating rate gives a fit to the time constant of

$$\tau \sim \hat{\gamma}_{MHD}^{-0.72} \gamma_h^{-0.28} \tag{6}$$

which agrees well with the analytic prediction given by Eq. (4).

In toroidal geometry, any non-axisymmetric magnetic harmonic that has a component of the magnetic field perpendicular to the axisymmetric flux surfaces at the harmonics rational surface causes a change in topology; that is, perturbations which satisfy

$$\vec{B}_{mn} \cdot \hat{n} = \vec{B}_{mn} \cdot \vec{\nabla}\psi_0 / |\vec{\nabla}\psi_0| \neq 0 \tag{7}$$

at the $q = m/n$ rational surface break topology and are termed "tearing-parity" modes. Modes which have zero resonant normal components are termed "interchange-parity" modes [6]. Due

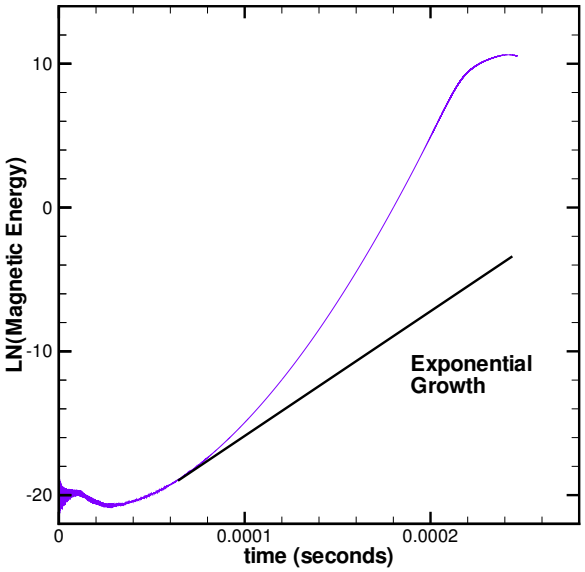

FIG. 3: The $n = 1$ perturbation grows faster than exponential as predicted by analytic theory.

to the frozen flux theorem, ideal instabilities necessarily are interchange-parity modes. As ideal instabilities grow in amplitude, they distort the flux surfaces, but not break the topology; therefore, cause no confinement degradation. The key to understanding disruptions caused by ideal instabilities is the mechanism by which resonant normal components of the magnetic field are generated in the presence of finite resistivity.

In Figure 5, the normal components of the dominant harmonics are plotted along with the safety factor for time $t = 0.217\ msec$. Note that these are calculated with reference to the new flux surfaces which have shifted due to the heating of the plasma (the magnetic axis has shifted 2 cm at this time). The safety factor profile is the same (within numerical accuracy) as the equilibrium profile which is consistent with no reconnection and the slow heating assumption of the flux-conserving tokamak [7]. At this time, the $n = 1$ perturbation is approximately 2 orders of magnitude smaller than the equilibrium toroidal field thus in the nonlinear regime. Even in the nonlinear regime, the harmonics have similar structure as the linear eigenfunctions, only scaled up to larger amplitudes. This explains the relatively good agreement of the GATO eigenfunctions and experimental comparisons even though the experiment is in the nonlinear regime[8].

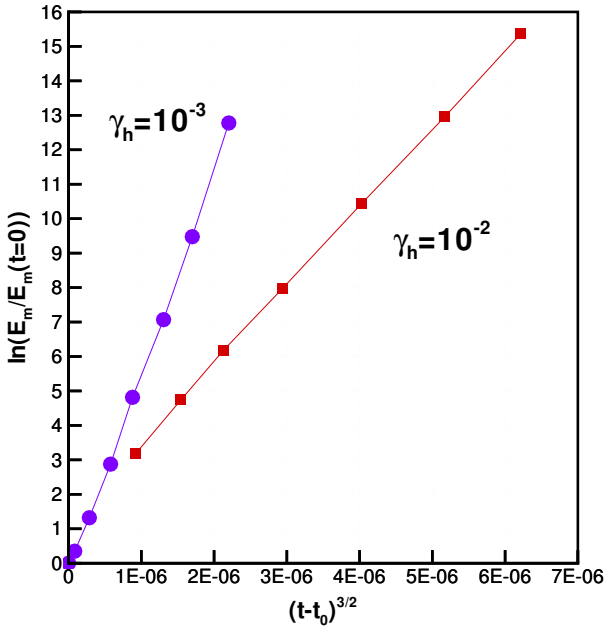

FIG. 4: Plotting the log of the magnetic energy, E_m, versus the the normalized time raised to $3/2$ power shows excellent agreement with the analytically-predicted scaling behavior as evidenced by the straight lines.

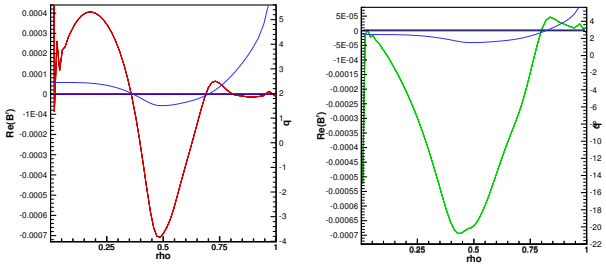

FIG. 5:

III. NIMROD SIMULATIONS OF DIII-D DISCHARGE 87009

To minimize the interactions of the hot plasma with the cold wall, modern tokamaks divide the plasma into two distinct regions: a core region where field lines close upon themselves thus confining the plasma ($T_e \sim 10keV$) in DIII-D) , and a "halo" region where the field lines intersect the wall and the plasma remains cold ($T_e \sim 10eV$ in DIII-D) as seen Figure 6. The separatrix which divides the two regions is only clearly defined with two dimensional magnetic fields – with three dimensional magnetic fields there is in general a stochastic region which tends to blur the

separation. Accurate modeling of the heat flux is required therefore to resolve the distinction between the halo region and core region as the plasma evolves nonlinearly.

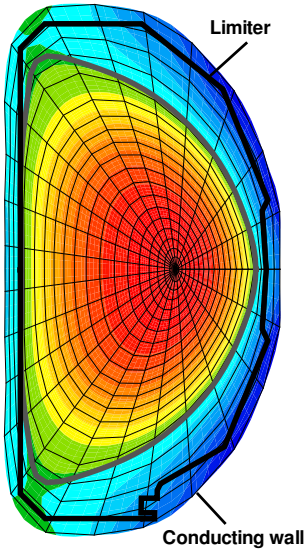

FIG. 6: In axisymmetric equilibrium, the plasma region contains a hot region where the field lines are closed and a cold, halo plasma where the field lines strike the wall. Dirichlet boundary conditions are applied at the vacuum vessel.

To simulate the nonlinear behavior of this discharge, the simulation was initiated from an equilibrium based on the best equilibrium reconstruction at $1675ms$. Because starting below the critical ideal MHD threshold add computational cost to an already expensive calculation, equilibrium pressure was raised self-consistently by 8.7% above the best equilibrium reconstruction to place the plasma beta above the ideal MHD threshold. The plasma equilibrium is shown in Figure 8, and a cross-sectional plot of the plasma is shown in Figure 6.

The simulations presented were run with a temperature dependent resistivity normalized such that the Lundquist number in the core plasma was $S = 10^5$. A ratio of $\kappa_\parallel/\kappa_\perp = 10^8$ was held constant throughout the computational domain. The boundary conditions are applied at the vacuum vessel (modeled as a perfectly conducting wall), and not the first material wall, as seen in Figure 6. The normal component of the magnetic field is held constant at the conducting surface. For the density, velocity, and temperature, the boundary conditions are also applied at the vacuum vessel instead of the more physical limiter surface. This is done for two reasons: 1) applying the "natural boundary conditions" at the limiter would give no density flux across the limiter, which is less physical than our current method of applying the natural boundary conditions at the vacuum vessel

and allowing a mass flux across the limiter; 2) On the time scales of the mode growth and nonlinear evolution, impurities would not have time to penetrate into the plasma. Thus, complicated plasma-wall interactions are unimportant for this simulation.

In Figure 7, the global parameters of internal energy and plasma current from the NIMROD simulation are shown. The plasma energy decrease by two-thirds in approximately 200 microseconds, in qualitative agreement with the experiment. Because constant voltage boundary conditions are used in this simulation, the plasma current changes as reconnection processes occur inside the plasma and the internal inductance changes. To explain the processes leading to the loss of energy confinement, a series of visualizations is presented. In Fig. **??**(b), the initial starting point of the NIMROD simulation is shown. The temperature isosurfaces show a reversed temperature profile due to the peaked pressure profile and broader density profile. Two magnetic field lines are shown, both colored according to the temperature with the brightness of the nodes indicating the distance along the fieldline. The fieldlines are initialized near each other, and at this early time are nearly on top of each other as they wind around the temperature (flux) surfaces. Finally, the DIII-D limiter wall, corresponding to the axisymmetric version of the black line shown in Figure 6, is shown with the heat flux contours shown upon it. At this early point in time, the heat flux is small and cannot be seen.

As the temperature evolves, the first notable macroscopic feature is the appearance of a $2/1$ island due to forced reconnection from the growth $3/1$ and $1/1$ perturbations at 441 microseconds into the simulation. As seen in Figure 9(a), at this time step, the temperature has equilibrated sufficiently that the island can be seen in the temperature isosurface, although significant variations of the temperature along the magnetic field line are beginning to occur. At this point in time, secondary islands are also forming near the separatrices and the edge region has already gone stochastic. (NOTE: Need to add a Poincare surface of section to both figures). At 579 microseconds into the discharge, the core region is largely stochastic as shown in Figure 9(b). As shown in the three dimensional figure, the two lines which began near each other diverge, and fill a large volume of the plasma with significant temperature variation along the fieldlines. The heat flux on the limiter is increasing as evidenced by the contour plots along the limiter wall.

At time of maximum heat flux, Figure 10(a), the heat flux is localized toroidal on both the top and bottom divertors 180 degrees apart. There is also a significant poloidal structure to the heat flux. Exploring the topology of the magnetic field in more detail, in Figure 10(b), we see that the locations of maximum heat flux are connected by a magnetic field line.

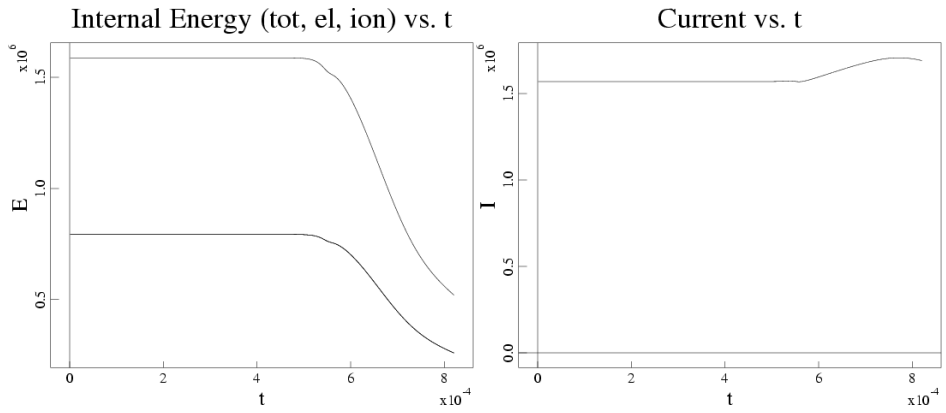

FIG. 7: In axisymmetric equilibrium, the plasma region contains a hot region where the field lines are closed and a cold, halo plasma where the field lines strike the wall. Dirichlet boundary conditions are applied at the vacuum vessel.

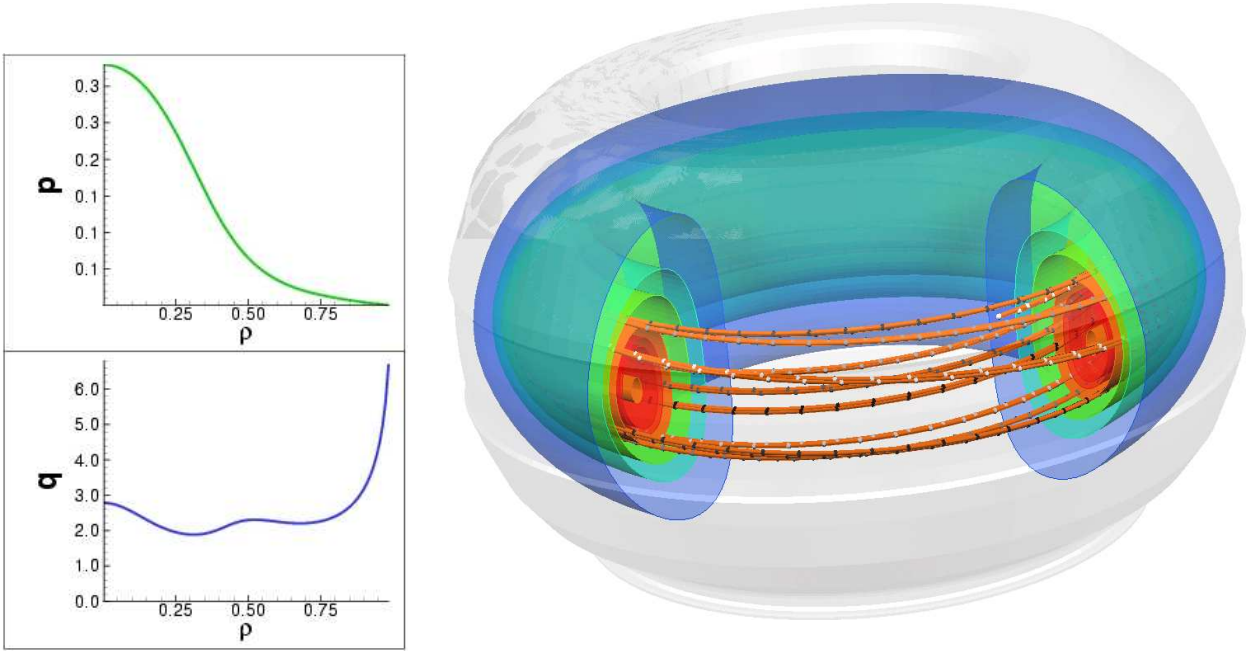

FIG. 8: (a) Equilibrium reconstruction of DIII-D discharge 87009 at $1675msec$ shows a reverse shear profile and peaked pressure profile. (b) The three dimensional plots of the simulation include temperature isosurfaces, magnetic fieldlines colored according to temperature, and the heat flux on the limiter.

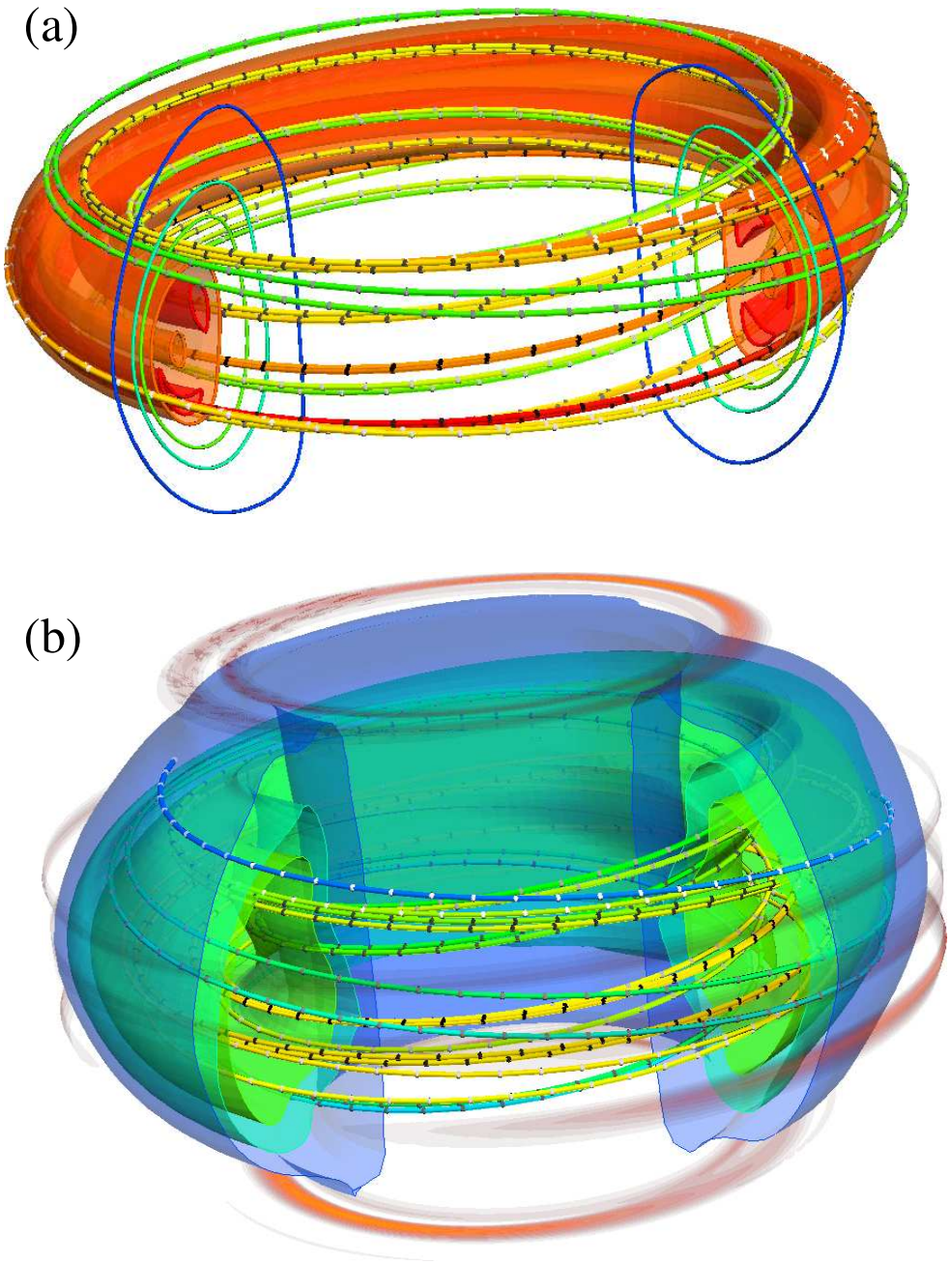

FIG. 9: In axisymmetric equilibrium, the plasma region contains a hot region where the field lines are closed and a cold, halo plasma where the field lines strike the wall. Dirichlet boundary conditions are applied at the vacuum vessel.

(a)

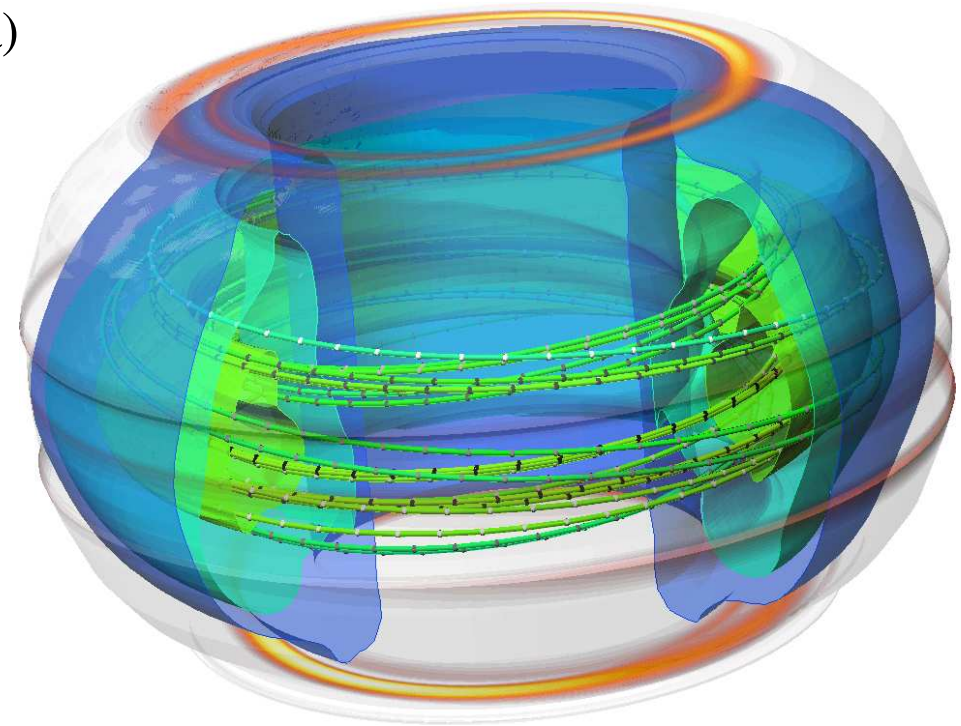

(b)

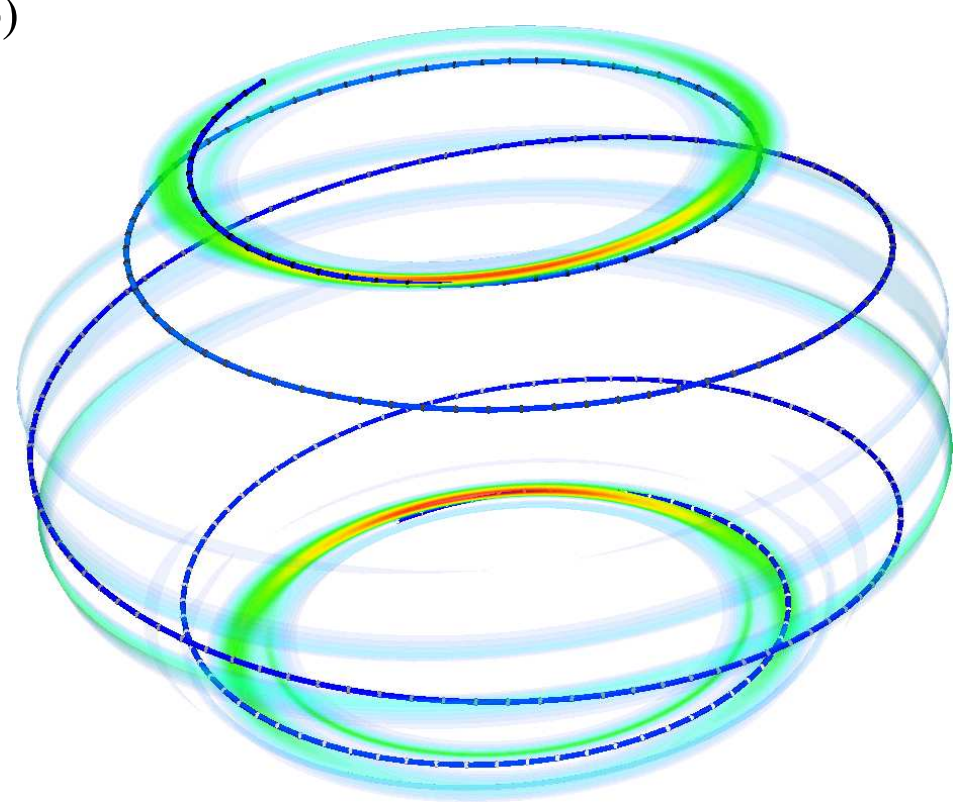

FIG. 10:

IV. DISCUSSION AND CONCLUSIONS

The fixed-boundary scale simulations proved difficult primarily due to the need to run at such large values of β due to the restriction of the conducting wall on the last closed flux surface which, combined with the high triangularity and ellipticity of this case, caused the plasma geometry to be very challenging. Despite the heuristic nature of the analytic derivation of mode growth being driven through an ideal marginal instability point, the NIMROD simulations show that the analytic scaling given by Eq. (3) gives an excellent description of the mode growth even into the nonlinear regime.

---

[1] J. Callen, C. Hegna, B. Rice, E. Strait, and A. Turnbull, Phys. Plasmas **6**, 2963 (1999).

[2] E. Strait, Phys. Plasmas **1**, 1415 (1994).

[3] A. Glasser (????).

[4] W. Newcomb, Annals of Physics **10**, 362 (1960), ideal_mhd.

[5] J. Comp. Phys. (2003), to be published.

[6] B. Coppi, J. Greene, and J. Johnson, Nucl. Fusion **6**, 101 (1966).

[7] R. Dory and Y.-K. Peng, Nucl. Fusion **17**, 21 (1977).

[8] A. Turnbull and et.al., in *Predictive Capability of MHD Stability Limits in High Performance DIII-D Discharges* (IAEA, 2000).